The Thesis Committee for Tushar Sharma
Certifies that this is the approved version of the following thesis :

THIN FILM NANOPOROUS SILICA AND GRAPHENE BASED BIOFUEL CELLS (iBFCs) FOR LOW-POWER IMPLANTABLE MEDICAL DEVICE APPLICATIONS

APPROVED BY
SUPERVISING COMMITTEE:

Supervisor:

Xiaojing Zhang

Thomas E. Milner

THIN FILM NANOPOROUS SILICA AND GRAPHENE BASED BIOFUEL CELLS (iBFCs) FOR LOW-POWER IMPLANTABLE MEDICAL DEVICE APPLICATIONS

by

Tushar Sharma, B. Tech.

Thesis

Presented to the Faculty of the Graduate School of

The University of Texas at Austin

in Partial Fulfillment

of the Requirements

for the Degree of

Master of Science in Engineering

The University of Texas at Austin

August, 2010

Dedication

I whole-heartedly dedicate my work to my beloved parents, who have been extremely supportive of me in all my endeavors.

Acknowledgements

I would like to acknowledge my parents, UT faculty and my friends who have been very supportive of me in pursuing my dream project at The University of Texas at Austin. I am highly indebted to numerous faculty members, including Dr. Marc Feldman, Dr. Thomas Milner, Dr. Mauro Ferrari, Dr. Pengyu Ren, Dr. Rodney S. Ruoff, Dr. John Pearce, Dr. Krishnendu Roy, Dr. Allen Bard, Dr. Sanjay Banerjee, Dr. Andrew Ellington and last but not the least, Dr. Xiaojing (John X.J.) Zhang and their respective students who have been very helpful with generous advise, resources, and guidance. I would also like to thank all my lab members at the Zhang Research group for their help and support. I am also thankful to the Biomedical Engineering Department and its staff members for all their help. Lastly, I would like to acknowledge all my lovely fellow graduate students and friends without whom, this project could not have succeeded.

July 15, 2010

Abstract

THIN FILM NANOPOROUS SILICA AND GRAPHENE BASED BIOFUEL CELLS (iBFCs) FOR LOW-POWER IMPLANTABLE MEDICAL DEVICE APPLICATIONS

Tushar Sharma, M.S.E.

The University of Texas at Austin, 2010

Supervisor: Xiaojing Zhang

This thesis describes the fabrication and characterization of an inorganic catalyst based glucose Biofuel cell using nanoporous (mesoporous) silica thin-film as a functional membrane. The desired use of nanoporous silica based biofuel cell is for a blood vessel implantable device. Blood vessel implantable Biofuel Cells (iBFCs) are subjected to higher glucose concentrations and blood flow rates. However, reduction in the implant thickness is critical for the intra-vascular implantable Biofuel cells. Platinum thin-film (thickness: 25 nm) deposited on Silicon substrate (500 μm) served as the anode while Graphene pressed on Stainless steel mesh (175 μm) was used as the cathode. Control experiments involved the use of surfactant-coated polypropylene membrane (50 μm) and Activated Carbon (198 μm) electrodes. Preliminary results show that nanoporous silica thin film (270 nm) is capable of replacing the conventional polymer based membranes with an increased power density output of as high as 10 $\mu W/cm^2$ under physiological conditions. *in-vitro* (5 $\mu W/cm^2$) and *in-vivo* (10 $\mu W/cm^2$) experiments demonstrate the potential of ultra-thin iBFCs towards powering future medical implants.

TABLE OF CONTENTS

LIST OF TABLES

LIST OF FIGURES

1. INTRODUCTION

Cardiovascular disease (CVD) is the number one killer in the US and worldwide [1]. The increasing age of the population, the obesity epidemic, the increased occurrence of diabetes and the increased survival of patients with diseases that lead to heart disease further magnify this serious health problem. The most recent American Heart Association (AHA) report paints a grim picture of the present and future of CVD [1]. Currently, over 70 million Americans suffer from CVD and the overall cost of health care in 2007 alone exceeded 430 billion USD. Consequently, there is an upsurge in the various novel implantable devices to diagnose, monitor, and treat cardiovascular disease [2-10]. Since most of these implantable devices need to work on a long-duration basis (>8 years), the spotlight has shifted towards the development of compact, efficient and low-power consuming implants. With the emergence of micro-electro mechanical systems (MEMS) based implantable devices [8, 11] fabrication of low-power devices can be realized. But for even the most low-power consuming devices, use of batteries is not considered to be a suitable long-term solution. Batteries are considered to be bulky for MEMS based implants and for bigger implants like artificial pacemakers, defibrillators, and insertable cardiac monitors, batteries provide limited life-span. Currently, these batteries are replaced on average every seven years (**Table1**), while the life span of the patient may be more than 20 years, resulting in unnecessary pain and increased cost to the patient. Further, there is a desire to piggyback newer devices such as heart failure warning

systems onto AICDs and pacemakers, yet the batteries used in these existing devices lack sufficient energy to allow the addition of newer devices.

Table1: Comparison of implantable devices and their Power Requirements. Courtesy: Medtronics

Model	Description	Voltage	Current	Battery Capacity	Estimated Life
Reveal DX	Insertable Cardiac Monitor	3.6 V	-	0.25 Ah	3 Yrs
Maximo	Single Chamber ICD	3.2 V	9.1 µA (pacing)	0.9 Ah	9 Yrs
Vitatron	Pacemaker	2.8 V	14.8 – 24.2 µA (pacing)	1.4 Ah	7-8 Yrs

Considering the disadvantages associated with existing battery technology, implantable Biofuel Cells (iBFCs) are attracting attention. iBFCs provide superior advantages over conventional batteries by reducing patient costs for battery replacements while simultaneously providing ease of sterilization and biocompatibility [14, 15].

Power source / Requirement	Biofuel cells	Biothermal converters	Mechanical converters	Nuclear generators	Batteries
Constant power output	s	w	o	s	s
Gentle energy transfer	s	s	t	n.a.	n.a.
Biocompatible	s	s	o	t	s
Sterilizable	s	s	s	s	s
Long term stable	o	s	o	s	s
Low patient risk	o	s	o	w	s
Power output ≥ 1 mW ?	w	w	o	s	s

Table 2: Comparison of various energy sources. Ref:[12, 13]; s: strength, w: weakness, o: opportunity, t:threat, n.a.: not applicable

Table 2 summarizes the advantages of an iBFC over other sources for energy generation. Realization of efficient iBFCs can circumvent existing hurdles and aid the development of next generation implantable devices and sensors [14].

1.1 Background

Implantable Biofuel Cells (iBFCs) have been a topic of interest since the 1970s [16-18]. These early efforts were motivated by the short life-time of the zinc/mercury oxide batteries commonly used at that time. Zinc/mercury oxide batteries were used to power cardiac pace makers, but they required frequent replacement. The power output of these first implantable Biofuel cells in the 1970s was in the range of 40 μW, sufficient to supply an ICD [19] (**Table1**). The capability of biofuel cells for powering an implantable artificial heart was also proposed and demosntrated [14, 20]. Although the durability of iBFCs when implanted outside the abdominal cavity exceeded 150 days [19], biocompatibility was not fully proven. However, following the introduction of the lithium iodine battery in 1972 [21], and the subsequent improvement of pacemaker battery lifetime, no further development of iBFCs have been reported. The rapid progress in autonomous, self-sufficient MEMS (micro-electro-mechanical systems) implants has revived the research in long-term stable sources of energy for implantable devices. Presently, very few research groups are working actively on iBFC [22, 23].

1.2 Biofuel Cells

In any fuel cell, electrical energy is generated by the electrochemical reaction of fuel and oxidant at two spatially separated electrodes [16], usually separated by an insulating membrane (**Figure 1**). Electrons, released upon the electro-oxidation of the fuel, travel from the anode through an external circuit to the cathode, where the terminal electron acceptor, usually oxygen, is reduced. The driving force of the electron flow is the difference in electrochemical potential of the anode and cathode redox pairs. The insulating membrane maintains electroneutrality inside the fuel cell compartments by facilitating ion diffusion (in an ionic electrolyte) between the anode and cathode.

In general, glucose-consuming fuel cells can be divided into three main types according to the type of catalyst that is used to enable the electrode reactions: *enzymatic, microbial, and a biotic glucose fuel cells*. Enzymatic fuel cells employ enzymes such as glucose oxidase and laccase in their isolated forms, whereas in microbial fuel cells the enzymatic system of a whole, electroactive micro-organism is used. In contrast, abiotically catalyzed fuel cells make use of non-biological, abiotic catalysts, e.g., noble metals or activated carbon. Over the last four decades, research in both the development of enzymatic and microbial fuel cells has been reported [24-26]. Whereas implantable enzymatic glucose fuel cells are currently under development, the

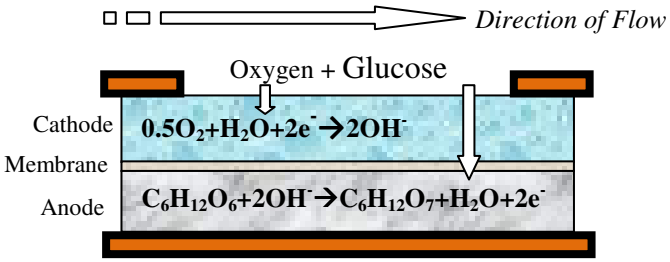

Figure 1: Schematic of a BFC

limited stability of enzymes renders their application in a long-term implantable fuel cell power supply problematic [27]. Power-supply systems based on microbial fuel cells are not seriously considered for implantation, due to the infective nature of most known micro-organisms and the associated risks herewith. Abiotically catalyzed fuel cells employ mainly noble metal catalysts and are therefore considered to be advantageous regarding their sterilizability, long-term stability, and biocompatibility [28].

Theoretically, glucose can be completely oxidized to carbon dioxide and water, releasing 24 electrons per molecule glucose [23]. The relevant fuel cell reaction and theoretical cell voltage would be given as:

Anode: $C_6H_{12}O_6 + 2\ OH^- \rightarrow 6CO_2 + 18\ H_20 + 24\ e^-$

Cathode: $6\ O_2 + 12\ H_2O + 24\ e^- \rightarrow 24\ OH^-$

Overall reaction: $C_6H_{12}O_6 + 6\ O_2 \rightarrow 6\ CO_2 + 18\ H_2O$

$\Delta G^\circ = -2.87 \times 10^6$ *J/mol[28];* $V^\circ = 1.24V$

Where, ΔG° is the standard Gibbs Free Energy and V° is the standard Reaction Potential.

In practice, the transfer of 24 electrons per molecule of glucose has not yet been achieved. Rao and Drake reported gluconic acid to be the only reaction product that could be identified [28]. The oxidation of glucose to gluconic acid only yields two electrons per molecule of glucose and the corresponding electrode reactions are given by:

Anode: $C_6H_{12}O_6 + 2\ OH^- \rightarrow C_6H_{12}O_7 + H_20 + 2\ e^-$

Cathode: $0.5\ O_2 + H_2O + 2e^- \rightarrow 2OH^-$

Overall reaction: $C_6H_{12}O_6 + 0.5\ O_2 \rightarrow C_6H_{12}O_7$

Where,

$\Delta G^\circ = -2.51 \times 10^5$ *J/mol[28];* $V^\circ = 1.30V$

Kerzenmacher *et. al.* [23] summarized various designs employed for testing BFCs. To simulate the physiological environment for testing a iBFC, glucose solution in PBS (pH=7.4) is commonly used. Literature also suggests addition of Polyox to simulate blood viscosity [43]. A common problem with the iBFCs targeted for human body implantation is the concomitant presence of glucose and oxygen and the lack of a glucose selective inorganic anode. For this purpose a significant effort has been directed toward the development of electrodes [29-34] or designs [35-40] to avoid oxygen interference on the anode. The most popular design to date is the sandwich type assembly of electrodes (**Figure 2**). The sandwich type assembly of iBFC works by depleting the oxygen concentration at the cathode, leaving glucose behind. Glucose must diffuse through the cathode to the anode where it gets oxidized. By designing a one-sided opening of such an iBFC, oxygen is depleted from the plasma entering the iBFC and minimal interference by oxygen is observed at the anode. A disadvantage of this system is that along with oxygen, the cathode and membrane also depletes the glucose flux due to steric hindrance to diffusing molecules.

1.2.1 SITE OF IMPLANT

In principle, an iBFC can either be directly in contact with the blood stream or implanted in tissue. The reactant supply of implantable fuel cells developed for tissue implantation [41, 42] relies solely on diffusion. While the surrounding tissue poses an additional mass transfer resistance, the risk of thrombi formation and blood coagulation is minimized compared to when exposed to blood stream. The placement site for such an iBFC is envisioned to be directly on the exterior surface of the pacemaker [29]. This site would facilitate implantation procedures and eliminate the risk of pacemaker lead failure, which was a common reason for pacemaker breakdown previously [19, 28].

In contrast, blood stream implantable iBFCs have been proposed [43]. The blood flow provides a steady reactant supply that is not limited by diffusion from blood vessel walls into the surrounding tissue. The glucose diffusion rate in the case of cylindrical electrodes embedded in the walls of blood vessels, which is replenished with fresh glucose by blood flow of 800-4000 mL/min, is expected to be as high as 1-2 mA/cm^2 [44]. Whereas the glucose diffusion rates for an iBFC implanted in tissue is less than 0.2 mA/cm^2 [19]. Hence, shifting the iBFC implant site from tissue to intra-vascular lumen can be highly advantageous for power generation. However, a blood stream implantable device must be designed so that blood flow is not impaired, and that no regions of reduced flow velocity are formed, which might increase the risk of thrombi formation. The employed materials must be compatible with blood, especially with respect to coagulation. An intravascular iBFC suffers from complications arising when having to surgically deploy the device into a major blood vessel. Implantation in the blood stream has therefore been considered

mainly in early studies, where the increased reactant supply posed a major factor to reach the final aim of powering an artificial heart [23].

1.2.2 ANODE

Apart from the commonly used platinum catalysts [45-47], other noble metals and alloys that are highly active for glucose oxidation have been reported. Most commonly used include platinum-ruthenium alloys, rhodium and iridium. Smooth platinum electrodes exhibited current densities up to 1μA/cm^2 before rapid irreversible polarization was observed, whereas smooth iridium, platinum-ruthenium (50 at% platinum), and rhodium could sustain current densities three, five and seven times higher, respectively [23, 48]. Recently a platinum-bismuth alloy on activated carbon, originally developed for the production of gluconic acid by direct chemical oxidation of glucose [48], has been reported as anode for an iBFC.

One of the most effective anodes reported was a special type of Raney-platinum catalyst developed at Siemens [49]. Ferrous metals and tungsten have been alloyed with platinum and subsequently removed from the alloy by chemical and electrochemical etching to create highly rough catalysts surfaces [50]. Platinum-tungsten, fabricated from an alloy containing additions to a conventional platinum black electrode in anaerobic phosphate buffer containing 2% (0.11 mol/L) glucose (1.1 mA/cm^2 after 24 h at 400 mV vs. the reversible hydrogen electrode) [23].

Glucose-selective noble metal alloys have been reported by Fishman [23]. He investigated glucose oxidation on platinum, gold-platinum, and gold-palladium (Pd< 50

at%) alloys and found that the addition of lead acetate to the plating solutions leads to electrocatalytic selectivity for glucose oxidation in neutral media containing dissolved oxygen. However, Kerzenmacher *et al* have reported that the above information was only presented in a conference proceeding and was devoid of details [23]. There is no record of follow up work or any other details.

1.2.3 CATHODE

Platinum showed the highest oxygen reduction performance in a comparative study including palladium, gold, and silver in isotonic phosphate buffer at neutral pH [14]. Although silver is considered to be insensitive towards glucose, its oxygen reduction onset potential is 400 mV more negative compared to platinum [23], which directly translates to lower fuel cell voltage and performance. Similar to silver, activated carbon has no affinity for glucose [23] and its oxygen reduction onset potential is only about 100 mV more negative compared to platinum. Hence activated carbon is a much more suitable cathodic material and has been widely used as the selective oxygen reduction catalyst in fuel cells employing an oxygen-selective cathode catalyst.

1.2.4 MEMBRANE

All of the designs for iBFCs proposed to date have relied on the use of polymer membranes as the diffusion barrier between the anode and cathode (**Figure 2**). The motive behind using polymer membranes is two fold: (1) the polymer membrane acts as an insulator between the conductive electrodes, and (2) the polymer membrane promotes glucose diffusion and resists oxygen diffusion from the cathode to the anode.

In the case of fuel cells employing an oxygen-selective cathode catalyst, the separator must not only be an ionic conductor but also allow for the diffusion of fuel and its reaction products to and from the anode. A variety of candidate materials have been reported. Among them, weak cation exchange hydrogels of Polyvinyl alcohol-polyacrylic acid cross linkages, glycolmethacrylate, cuprophane, sulfonated PTFE membranes, dialysis and cellulose membranes, the latter also soaked with poly(vinyl alcohol) (PVA) [17, 19, 23]. Hydrolysis or oxidative effects of hydrogels based on poly(vinyl alcohol)-poly(acrylic acid) (PVA-PAA) and glycolmethacrylate were observed when they were disconnected after prolonged fuel cell operation [23].

1.3 CURRENT OUTLOOK

A common problem with iBFCs is the lack of an inorganic catalyst that can selectively oxidize glucose from blood. Presence of oxygen in blood interferes with glucose oxidation at the anode. Hence a significant effort has been expended to develop anodic materials for sandwiched-electrode design (**Figure 2b**), which consumes oxygen at the oxygen-selective cathode, leaving glucose for oxidation at anode. Little attention has been diverted to the membrane itself. A common problem with all of the polymer membranes is the random polymerization and casting process, which leads to a very high variation in the pore sizes and physical properties at the molecular level. The pore sizes in the range of 5 nm – 12 nm for the various membranes has been used for iBFCs [19]. This problem can be circumvented by using nanoporous (mesoporous) silica in place of polymer membranes. The advantages of using nanoporous silica surpass the polymer

membranes used, in terms of controllable pore size, pore distribution, surface properties (hydrophobicity and hyrdophilicity), thickness, ease-of-fabrication, and sterilization.

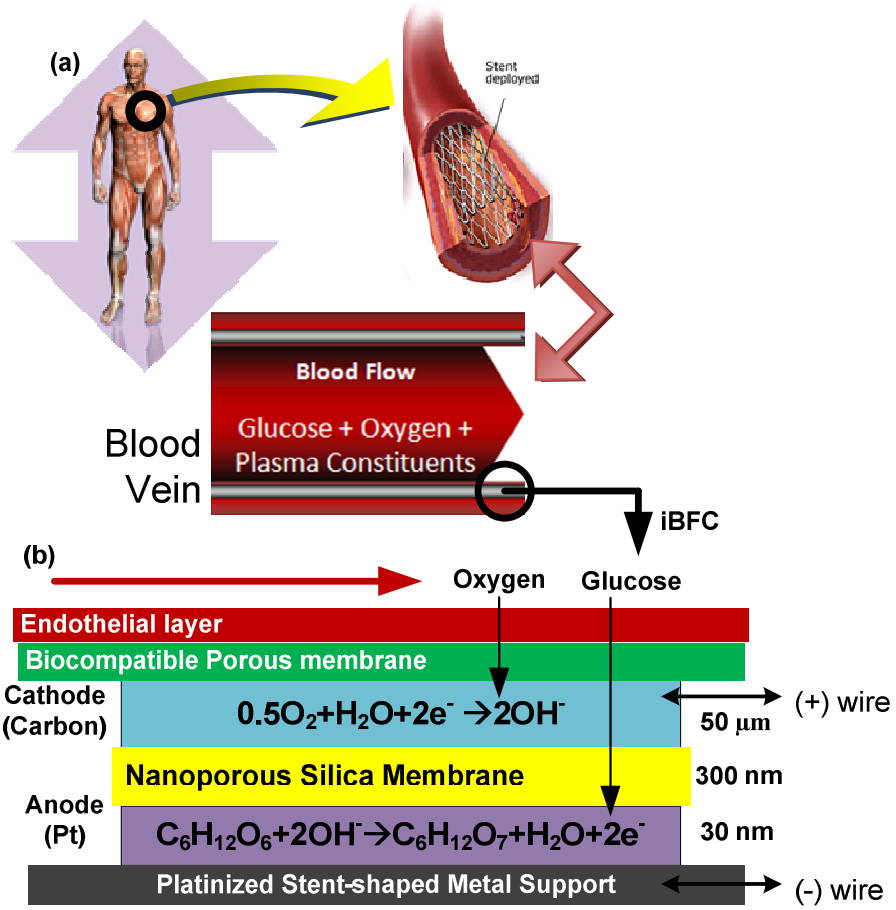

Figure 2: (a) Long-term vision for an iBFC, (b) Cross-section with approximate thickness of the different components, showing the working principle of a functional iBFC

Controlling the pore size and surface properties of the nanopores (hyrdrophilicity) will allow mimicing the polymer membranes used for iBFC. Further, membrane thickness can be drastically reduced for higher diffusion rates [43].

Hence, the long term aim is to enable creation of efficient, ultra-thin implantable Biofuel

Cells (iBFCs) which can be mounted on stents and deployed in veins (**Figure 2**). This can be achieved in two different ways: (1) Use of novel catalysts and materials for efficient energy generation, and (2) Shift the implant site from sub-clavicular skin pouch to an intra-venous implant. Reduction in thickness of present iBFCs is critical for safe and efficacious intra-venous implants**.**

For the present project, ***we focus on the development of ultra-thin nanoporous (NP) silica membranes to limit oxygen competition and are compatible with deployment on a venous stent.*** We also present a method to develop an integrated NP Silica-anode component for an iBFC. Since the NP silica does not absorb water, delamination is prevented. We envision a stent that is the anode itself and the remaining layers be added on top of the anode. However, development of the completely optimized iBFC structure would require optimization of the cathode as well, which is beyond the scope of the present project. Thin cathodes, made by black-Pt deposition on gold coated porous membranes, could be used for testing existing iBFCs [51]. If successful, this would mark a milestone to embark on for cathode optimization to end in complete iBFC design which can then be transferred to a stent-shaped support.

The motivation for use of ultra-thin nanoporous (mesoporous) silica as the membrane is two-fold: (1) provide well controlled physio-chemical properties of the nano-pores (shape, size, distribution) for enhanced diffusion; and (2) drastically reduce the overall thickness of the iBFC. Since the problem associated with the use of blood plasma as an electrolyte is diffusional in nature, reduction of the membrane thickness would also help

boost the efficiency of the iBFC by reducing the path-length of the glucose molecules [43]. Combining the above mentioned strategies, we have assembled a highly efficient, ultra-thin iBFC.

2. EXPERIMENTAL SECTION

2.1 ELECTRODE FABRICATION

Anode was made of Platinum thin-film (thickness: 25 nm), e-beam evaporated on a commercial silicon wafer (500 µm, $\rho < 0.05$ Ω-cm). The silicon wafers were then diced to 5 x 5 mm^2 anodes. Contact angles of anode surface were measured by a goniometer using a captive bubble contact angle measurement. **Cathode** was constructed of chemically reduced graphene oxide as reported elsewhere [52]. Graphite oxide obtained using a modified Hummers method was reduced and filtered. The agglomerates of graphene sheets were assembled into electrodes by mixing with 5% polytetrafluoroethylene (PTFE) binder and rolled into 65 µm thick sheets. Activated carbon (Norit Super 30) was used as the control for comparison with graphene based electrodes. PTFE was used as the binder for activated carbon electrodes as well. The thickness of the activated carbon sheets was 210 µm. The electrodes were soaked in phosphate buffered saline (PBS, pH 7.4) solution overnight, prior to use in biofuel cell assemblies. When not in use, the electrodes were stored in PBS under vacuum.

2.2 PREPARATION OF THIN-FILM NANOPOROUS SILICA ON ANODES

Thin-film Nanoporous silica on anode was fabricated as shown in **Figure 3**, reported elsewhere [55, 57]. 14 ml of tetraethyl orthosilicate (TEOS) was dissolved in a mixture of 15 ml of ethanol, 6.5 ml of distilled water, and 0.3 ml of 6M HCl and stirred for 2 hours at 75°C to form a clear silicate sol. Separately, 1.2 g of L64, a tri-block copolymer

surfactant, was dissolved in 30 ml of ethanol by stirring at room temperature. The coating solution was prepared by mixing 10 ml of the silicate sol into the triblock co-polymer solution followed by stirring of the resulting sol for 2 hours at room temperature.

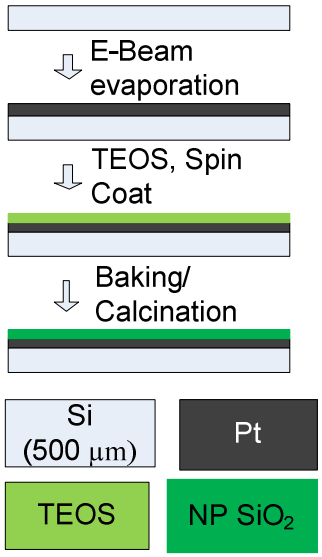

Figure 3: Schematic showing nanoporous silica fabrication

The pH of the mixture solution remained around 1.5. The coating sol was deposited on a platinum coated silicon (1 0 0) wafer by spin-coating (2000 rpm) for 20 seconds. To increase the degree of polymerization of the silica framework in the films and to further improve their thermal stability, the as-deposited films were heated at 80 °C for 12 hours in an oven. The films were calcinated at 425°C to remove the organic surfactant. The temperature was raised at a heating rate of 1°C per min, and the furnace was heated at 425°C for 5 hours. The resulting NP silica films were transparent and without cracks. Oxygen plasma ashing was performed in a Plasma Asher (March Plasma System) to pre-

treat the chip surface. The treatment was carried out with an O_2 flow rate at 80 sccm (standard cubic centimeters per minute) and a power of 300 W for 10 minutes. The NP silica coated anodes were then diced in to 5 x 5 mm^2 or 5 x 10 mm^2 sizes for *in-vitro* and *in-vivo* experiments respectively.

2.3 CHARACTERIZATION TECHNIQUES FOR NANOPOROUS SILICA

Details of characterization techniques used here have been reported elsewhere [55, 57]. Several characterization techniques were utilized to study the spin-coated nanoporous silica thin films. A variable angle spectroscopic ellipsometer (J. A. Woollam Co. M-2000DI) and WVASE32 modeling software was used to measure the film thickness and their porosity using the Cauchy model and the Effective Medium Approximation (EMA) model, respectively. Ellipsometric optical quantities, the phase (Δ), and amplitude (ψ) were carried by recording spectra for 65°, 70°, and 75° incidence angels using wavelengths from 300 to 1600 nm. In the Cauchy model, the top layer's thickness and reflective index were determined by fitting experimental data with the model and minimizing the mean square error. Using the EMA model, the films' porosities were calculated by assuming a certain volume of void in the pure silica and setting the top layer's thickness obtained by the Cauchy model as a constant. Transmission electron microscopy (TEM; FEI Technai; FEI Co.) was used to obtain micrographs of the plane view of the porous silica thin films at a high tension of 200 kV. N_2 adsorption/desorption analysis was used to measure surface area and pore size distribution. Quantachrome was used to record the N_2 adsorption/desorption isotherm at 77 K on the full range of relative

P/P_0 pressures. Brunauer-Emmett-Teller (BET) surface areas were determined over a relative pressure range of 0.05 to 0.4. Nanopore size distributions were calculated from the desorption branch of the isotherms using the Barrett-Joyner-Halenda (BJH) method with interconnecting channels. Contact angles of film surface were measured by a goniometer using the captive bubble contact angle measurement.

For testing the effect of sterilization on NP silica films, the fabricated NP silica anodes were placed in PBS and autoclaved at 121℃ and 15 psi. Following this, the NP silica anodes were removed and compared with non-autoclaved NP silica anodes using TEM imaging and a variable angle spectroscopic ellipsometer as described above.

2.4 ASSEMBLY OF *IN-VITRO* iBFC

Three types of iBFC were assembled as described in **Table 3**. **Figure 4** shows the schematic of the BFCs assembled. For the polymer membrane based BFC, a surfactant-coated polypropylene membrane (25 µm, average pore size: 64 nm, Celgard 3501) was placed between the electrodes. The porous membrane acted as the insulator while simultaneously providing glucose diffusion across the membrane.

Table 3: Description of the components of different types of iBFC tested in the present study

Label	Anode	Membrane	Cathode
Pt/PP/AC	Pt on Si wafer	Surfactant coated polypropylene	Activated carbon
Pt/PP/G	Pt on Si wafer	Surfactant coated polypropylene	Graphene
Pt/NP/G	Pt on Si wafer	Nanoporous Silica	Graphene

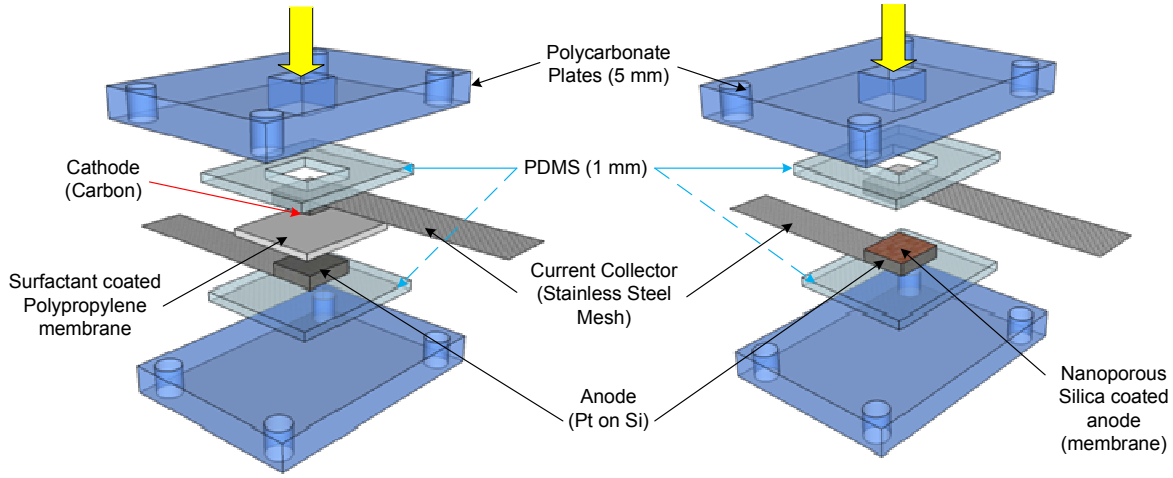

Figure 4: Schematic for setup of BFC (Biofuel Cell) for testing Nanoporous silica

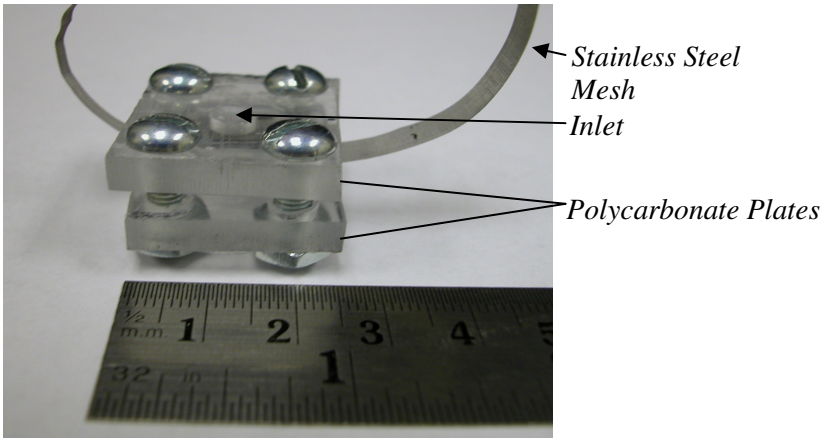

Figure 5: Packaged Biofuel Cell (BFC)

Stainless steel 316 (Wire Diameter: 0.23 mm, Square Size: 1.0 mm, Percentage of Open Area: 67.2%) was used as the current collector for the electrodes. Since the anode is comprised of conductive silicon, which is non-catalytic in nature [53], the stainless steel mesh based current collector (160 µm) was placed directly beneath the Pt/Si anode.

For the cathode, chemically reduced graphene oxide or activated carbon was manually pressed onto the stainless steel mesh. Thicknesses of all the electrodes are compiled in

Table 5. The electrodes were stacked as shown in **Figure 4**. Polydimethylsiloxane (PDMS) sheets with thickness (1-2 mm) provided mechanical support to the silicon anodes while damping the pressure effects due to the clamp. The packaged Biofuel Cell is shown in **Figure 5.**

2.5 ELECTROCHEMICAL TESTING

iBFC were assembled as described above and placed inside a glass beaker containing 0.1% or 0.42% glucose solution dissolved in phosphate-buffered saline solution (pH 7.4). Possible air trapped inside the BFCs was removed by placing the glass beaker under vacuum for 15 mins. The setup was then placed on a hot plate at 37 ˚C with continuous stirring to simulate physiological conditions. Throughout the experiments, the solution was continuously aerated. To measure the load characteristics of the assembled biofuel cell, the terminals were connected to a variable external resistance (0-12 kΩ), as shown in **Figure 6** and **7.**

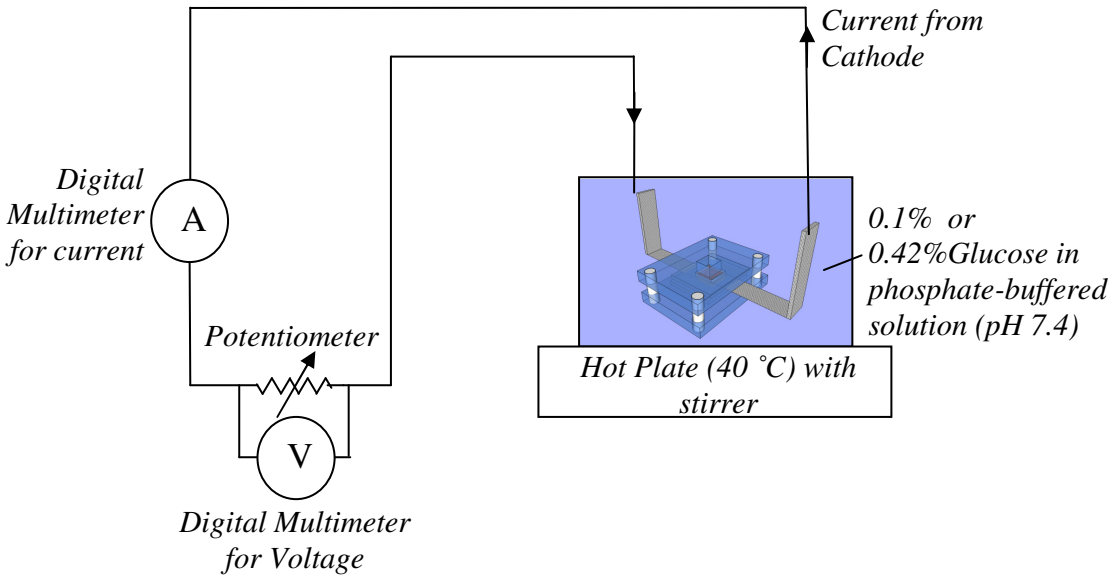

Figure 6: Experimental Setup for Biofuel Cell load characterizations

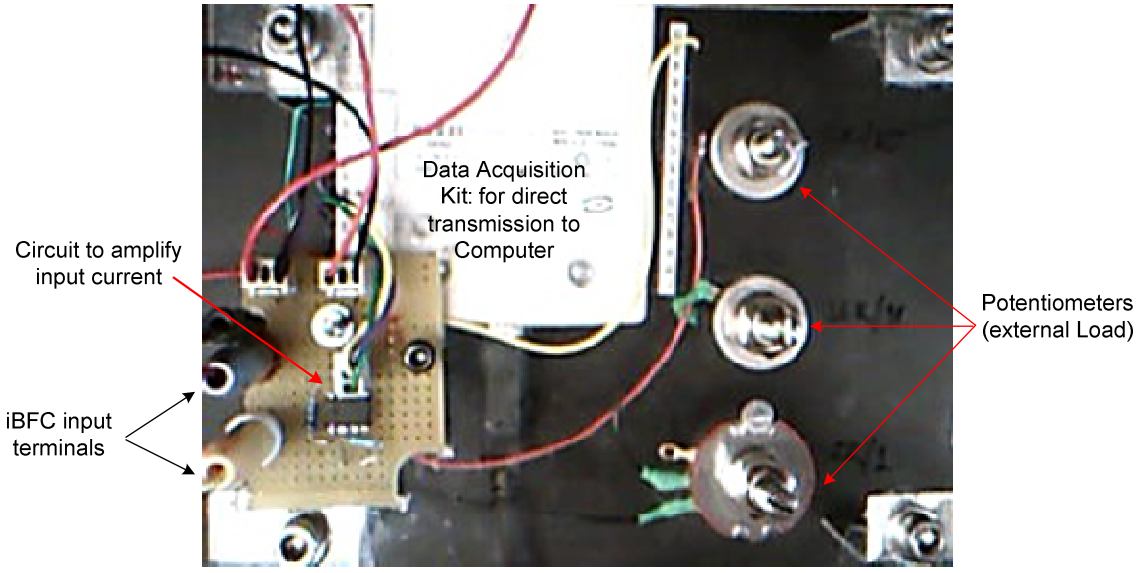

Figure 7: Photograph of a DC Load Box

To verify any affinity of the stainless steel mesh towards glucose oxidation, cyclic voltammetry was done using the CH Instruments facility at the Center for Electrochemical Research, the University of Texas at Austin. Stainless steel 316 mesh (Wire Diameter: 0.23 mm, Square Size: 1.0 mm, Percentage of Open Area: 67.2%) was used as the working electrode and a carbon rod was the counter and reference electrode. Results obtained from stainless steel mesh were compared with platinum wire (99.99%, 2 mm diameter).

2.6 ASSEMBLY AND IMPLANTATION OF THE *IN-VIVO* IBFC

These experiments were done at the University of Texas Health Science Center at San Antonio (Protocol Numbers: 09071-10-02-B1; 73-02-B1). For *in-vivo* experiments, the 10 x 5 mm^2 NP silica coated anodes were used to assemble the iBFC. Graphene pressed on platinum coated stainless steel mesh was used as the cathode. The two electrodes were carefully pressed between two polycarbonate sheets (13 x 5 x 1 mm^3). Polycarbonate sheets were locked in place temporarily using stainless steel screws. The platinum coated stainless steel mesh protruding from the iBFC was rolled into wire-form and covered using thermoplastic glue. Alligator clips were used to connect the tip of rolled stainless steel mesh to the external load (as described above). Assembled iBFCs were placed in PBS solution and vacuumed for 15 mins. iBFCs were then stored in PBS till the actual implantation.

For implantation inside the heart, a purse-string suture was tied to the anterior wall of the right ventricle in a Yorkshire pig. An incision was made directly through the right

ventricular myocardium. The iBFC was inserted into the right ventricular chamber and the purse-string closed to maintain hemostasis. In the second *in-vivo* experiment, the device was inserted in the right atrium of the pig to minimize the blood flow disruption. **Figure 8** shows a view of the open heart surgical preparation with the wire leads coming out from the atrium after implantation. The pigs were later sacrificed using standard and humane euthanasia procedures.

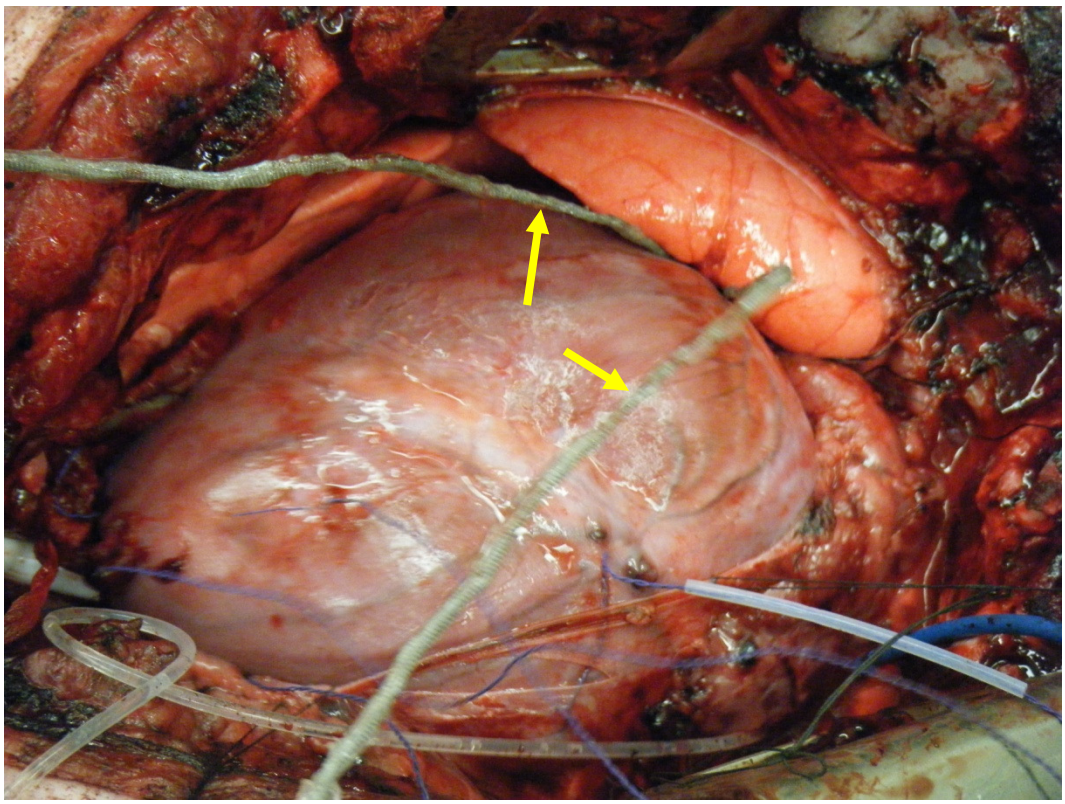

Figure 8: Photograph showing the iBFC implanted inside the swine heart (in Right Auricle) with Stainless Steel mesh-wires coming out (marked by arrows)

3. RESULTS

3.1 NANOPOROUS SILICA

Using a spectroscopic ellipsometer, tested thin film thickness and porosity was measured to be 281.816 ± 7.46 nm and 44.8815 ± 0.125%. In Figure 9, the TEM image of the plane view of the nanoporous silica thin film depicts a worm-like nanostructure overlying the porous layer. In **Figure 11**, N_2 adsorption/desorption curves were generated using a Quantachrome Autosorb-3b BET Surface Analyzer (inset) and the pore size distribution (3.2nm) was calculated using the Barrett-Joyner-Halenda (BJH) method. The adsorption/desorption isotherms describe a Type IV isotherm with a H_2 hysteresis loop (sloping adsorption branch and nearly vertical desorption branch), indicating a nanoporous silica structure with interconnecting channels. Inflection points appearing at $0.40 < P/P_0 < 0.75$ in Figure 11 indicated the formation of an ink-bottle shape nanopores. Samples of NP Silica obtained after autoclaving did not show any changes in the structure or thickness of the Nanoporous silica observed by SEM imaging and Ellipsometry, proving the process was suitable for standard sterilization in a clinical setting (Data not shown).

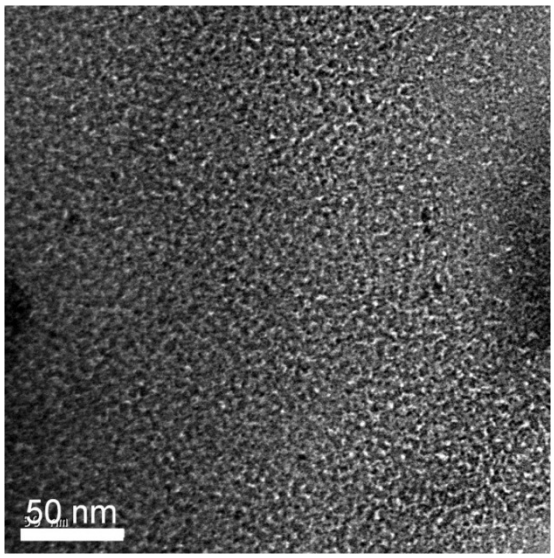

Figure 9: TEM image of porous silica thin films prepared using Pluronic L64. Courtesy of: Dr. Ye Hu (Dr. Ferrari's Lab)

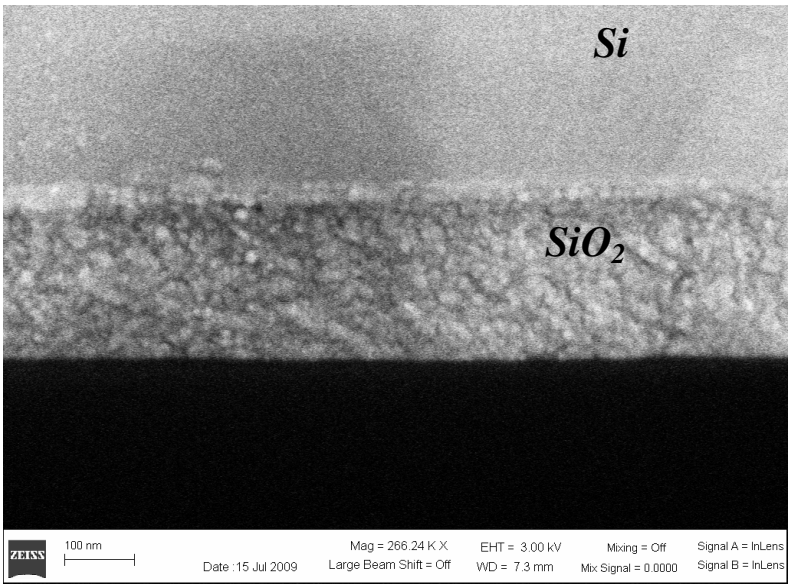

Figure 10: SEM image of the cross section of porous silica thin films prepared using Pluronic L64, showing the distinct Si crystal lattice and amorphous silica. Sandwiched platinum layer (25 nm) is not visible in this image.

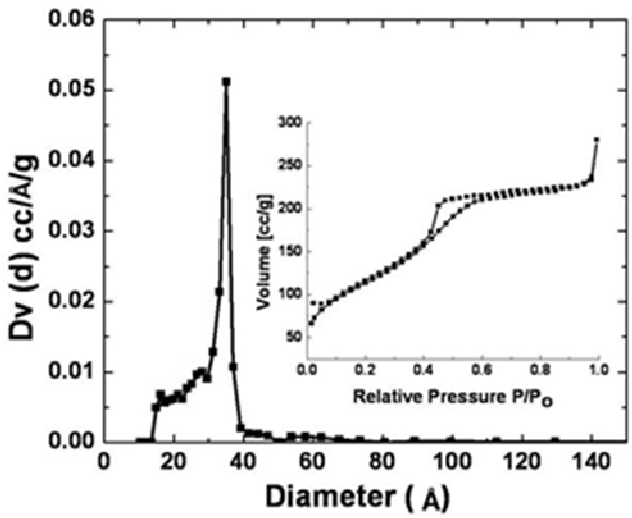

Figure 11: N_2 adsorption/desorption analysis (pore size distribution and isotherms in the insets), of the porous silica thin films prepared using Pluronic L64. Courtesy of: Dr. Ye Hu (Dr. Ferrari's Lab)

Contact Angle measurements showed that the platinum deposited on silicon wafer was strongly hydrophobic, which was not expected [54]. Metal surfaces have been known to be hydrophilic in general. The metallic surface might show hydrophobic properties due to the residual hydrogen atoms bound to the platinum atoms. However, having a hydrophobic metal surface might have aided assembly of nanoporous silica, which was previously coated on hydrophobic silicon surface [55].

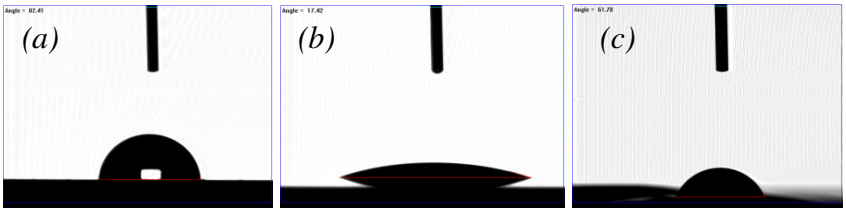

Figure 12: Contact angle measurements showing the water-surface contact angles for: (a) Platinum deposited on Silicon wafer, (b) NP silica on Pt/Si anode; and (c) Surfactant coated polypropylene membrane. The values have been summarized in Table 4. Courtesy of: Dr. Ye Hu (Dr. Ferrari's Lab)

Surfactant coated polypropylene was found to be hydrophobic as well. Polypropylene is well-known to show hydrophobic behavior by virtue of the carbon chains constituting the polymer. However, the membrane is surfactant coated for rapid wetting purposes, making it hydrophilic. The results suggest that the surfactant coating might have degraded with time changing the membrane surface from hydrophilic to hydrophobic. Hence, the stability of the surface coating is also a major concern for long-duration implantable applications. Nanoporous silica coating was found to have a stable shelf life in other studies [56, 57].

Table 4: Summary of the various contact angles for different surfaces used in the experiments.

Component	Contact Angle	Hydrophobic/Hydrophilic
Pt (25 nm) deposited on Si wafer	82.41	Hydrophobic
NP Silica on Pt (25 nm) deposited on Si wafer	17.42	Hydrophilic
Surfactant coated Polypropylene membrane	61.70	Weak Hydrophobic

3.2 BIOFUEL CELL PERFORMANCE

3.2.1 STAINLESS STEEL AS CURRENT COLLECTOR

Literature suggest the use of Platinum mesh as the most preferred current collector [23]. However the costs associated with platinum mesh forced us to seek for other alternatives.

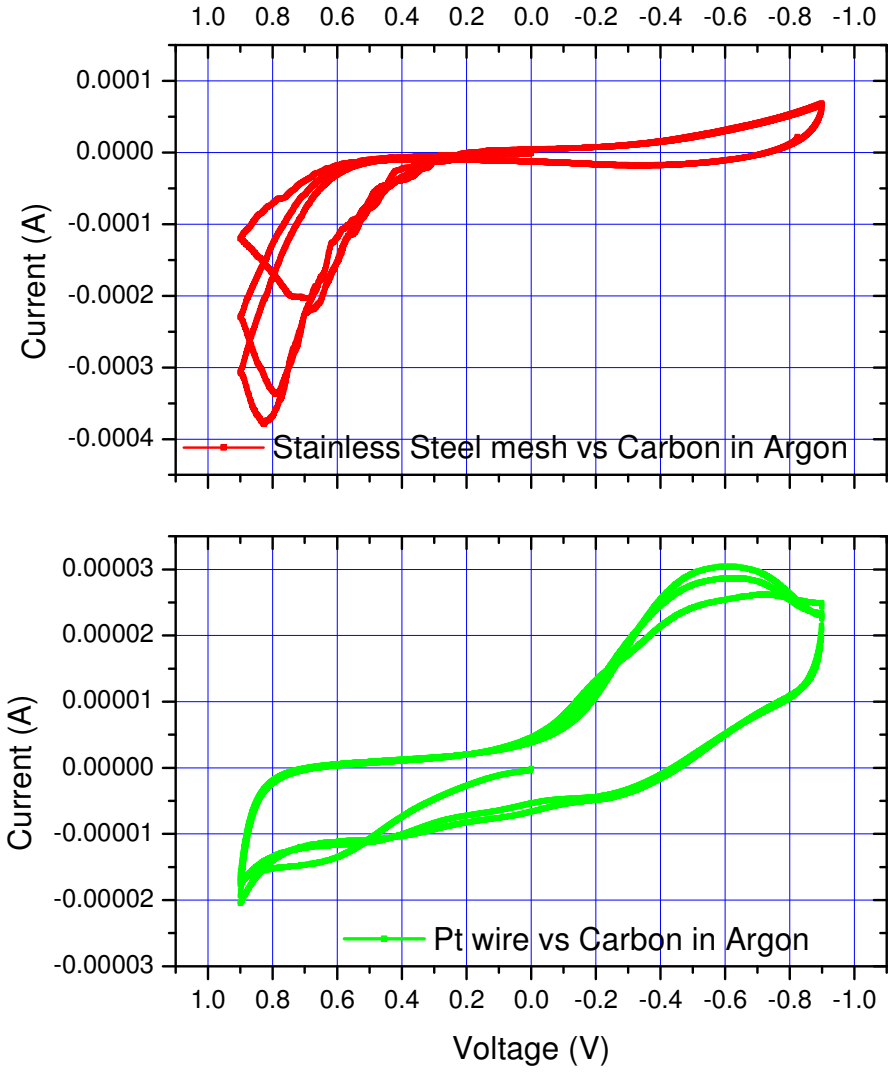

Figure 13: Cyclic Voltammetry graphs of Stainless Steel Mesh and Pt Wire showing that Stainless Steel mesh has no affinity for glucose and hence is a suitable current collector material

Stainless Steel is known for its stability and biocompatibility [58]. However, no published information is available on the use of stainless steel mesh as a current collector for biofuel cells. Hence, cyclic voltammetry experiments were done to check for the glucose affinity to stainless steel mesh. **Figure 13** shows the obtained data from cyclic voltammetry of stainless steel mesh versus platinum wire where carbon rod was used as the counter and the reference electrode. From **Figure 13** we observe that there was no glucose oxidation peak observed in the case of stainless steel mesh as was in the case of platinum wire (0.4 V). Further, oxygen reduction can be observed in Pt wire (-0.6 V). However, the oxygen reduction is prominent in the case of Platinum, indicating the higher affinity of platinum towards oxygen. From these results, it can be concluded that stainless steel mesh can be a good current collector as it would not introduce any error which can be due to oxidation of glucose on stainless steel mesh. More tests need to be done with better controls and reference electrodes to confirm this. However while all the studies reported use a platinum mesh, we have used stainless steel mesh as the cathodic current collector in the present study for consistency.

3.2.2 PERFORMANCE AT 0.42% GLUCOSE

Power density and polarization curves for the two BFCs have been plotted in **Figure 6**. From **Figure 6a**, it is clear that the replacement of activated carbon with graphene as the cathode can deliver high power densities (Pt/PP/G: 5 $\mu W/cm^2$). Hence graphene acts as a better cathode in place of activated carbon (Pt/PP/AC: 3.24 $\mu W/cm^2$). Further, the open circuit potential (OCP) of graphene based BFC (Pt/PP/G: 0.261 V) was higher compared to the OCP of activated Carbon based BFC (Pt/PP/G: 0.234 V). The power densities reported in the present study obtained from activated carbon (Pt/PP/AC: 3.24 $\mu W/cm^2$)

based BFC are higher than the values reported from similar studies (~2 μW/cm^2) [48]. Higher power densities may be attributed to higher glucose concentrations used to compensate for the presence of oxygen at atmospheric pressure conditions.

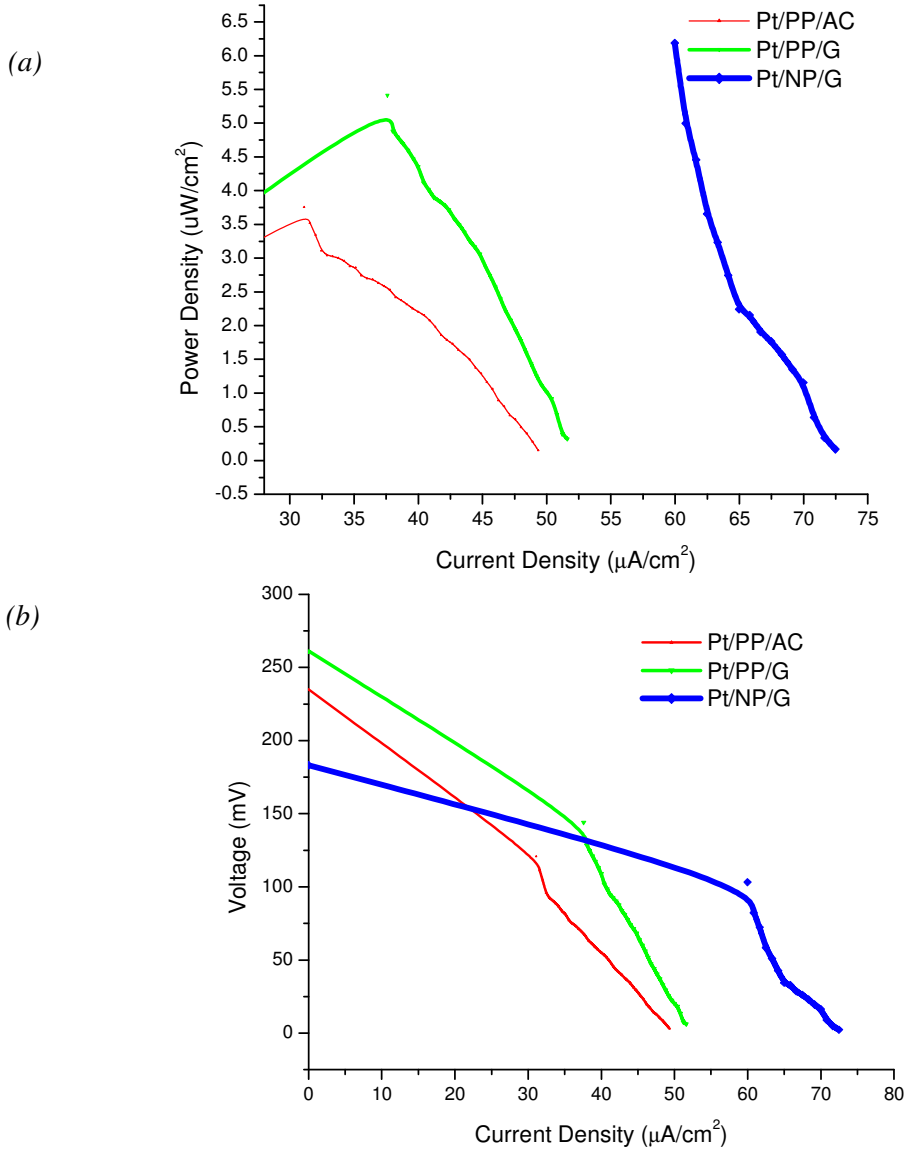

Figure 14: Experimental results obtained with Polymer membrane vs. Nanoporous Silica based BFCs: (a) Power Density Curves, and (b) Polarization Curves

NP silica based iBFC (Pt/NP/G) is capable of delivering higher power densities (6.23

$\mu W/cm^2$) than the polymer membrane based iBFC (Pt/PP/G: 5 $\mu W/cm^2$). The lower OCP obtained using NP silica based iBFC (Pt/PP/G: 183.2 mV) indicates the presence of oxygen at the anode. The absolute values of polarization recorded are very low compared to the reported literature values [48]. This is an indication of the possible interference of oxygen at the anode which in turn, could be due to inadequate clamp pressure from the polycarbonate sheets as well as diffusion of oxygen through PDMS. Further, this could also possibly be due to the presence of residual air in graphene that was not removed during vacuuming. The polarization values were found to improve with time, however. Better BFC designs for the presented electrode system should avoid the observed low polarization values for the two BFCs.

3.2.3 PERFORMANCE AT 0.1% GLUCOSE

0.1 % glucose is reported the physiological glucose concentration. Pt/NP/G iBFC (5.3 $\mu W/cm^2$) shows higher power density compared to Pt/PP/G iBFC (2.1 $\mu W/cm^2$) indicating better performance of the iBFC when the polypropylene membrane was replaced with nanoporous silica membrane. ***Figure 15*** shows the comparison of the power densities and polarization values obtained from the various iBFCs assembled. Appleby *et. al.* [15] have reported that introduction of oxygen causes an appreciable change in the open circuit potentials; there is minimal effect on the polarization curve. Pt/NP/G shows significantly higher open circuit potential (314.6 mV) compared to Pt/PP/G (181.4mV) and Pt/PP/AC (160 mV) while both the iBFCs show similar ohmic losses, determined by the slope of the curves.

(a)

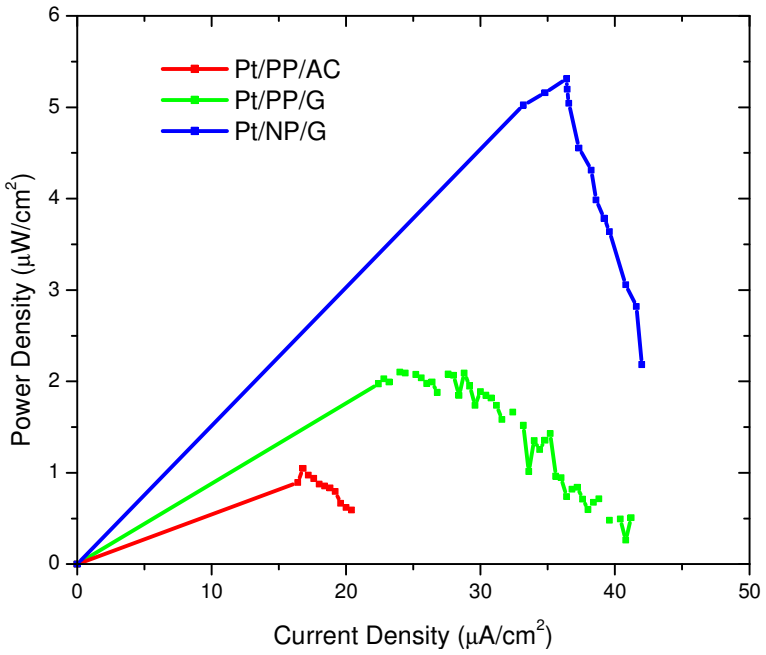

(b)

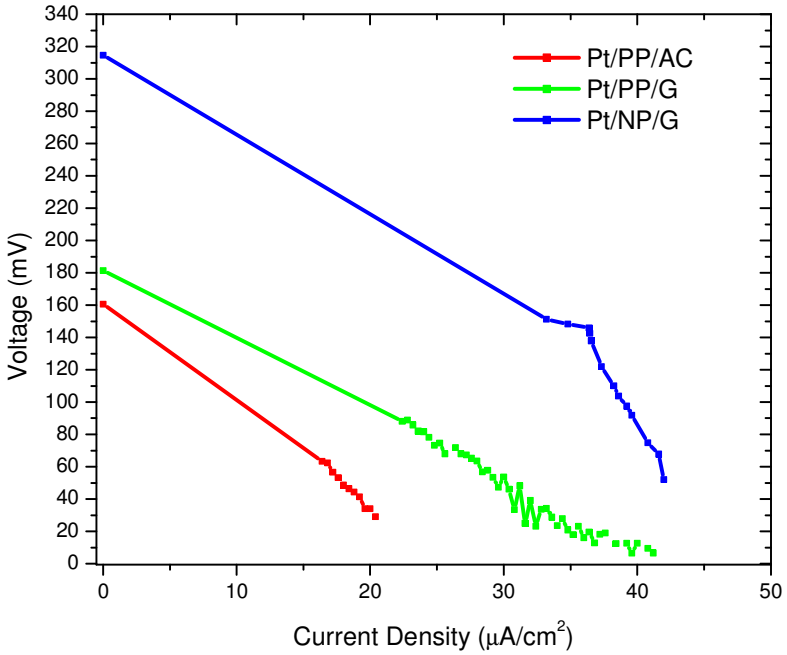

Figure 15: Experimental results obtained with Polymer membrane vs. Nanoporous Silica based BFCs: (a) Power Density Curves, and (b) Polarization Curves

An irreversible polarization change was observed upon disruption or change of operating conditions including changing of electrolytes as reported earlier [23]. Hence, long-term experiments (> 48 hours) could not be recorded.

Qu proposed that oxygen reduction in activated carbon occurs at the edges of the graphene layers that make up the structure of activated carbon whereas the micropores may not be used for oxygen reduction [59]. Graphene based cathodes used in the present study contain several graphene layers bound together using PTFE. Activated carbon based cathodes on the other hand contain several amorphous activated carbon granules bound using PTFE. Hence, only a fraction of the whole activated carbon granule surface would be chemically active. Graphene as a cathode shows considerable increase in performance (2.1 $\mu W/cm^2$) compared to similar setup based on activated carbon (1.1 $\mu W/cm^2$) in the present study.

3.3.4 COMPARISON OF PERFORMANCE

All the iBFCs operated at 0.1% glucose solution showed lower power density compared to 0.42% glucose solution. Lower power density was mainly due to the lower glucose concentration used (0.1%) and better represents the physiological glucose values. The presence of oxygen also had a visible effect on the open circuit potential of the iBFCs, which was lower for the iBFCs in the present study. Important values have been summarized in **Table 5**.

3.3.5 COMPARISON OF PERFORMANCE WITH OTHER REPORTED LITERATURE RESULTS

Table 5: Comparison of some iBFC performance with their components and operational conditions

Anode (µm)	Membrane (µm)	Cathode (µm)	Glucose concentration (% w/v)	Oxygen concentration (% w/v)	Max. Power Density (µW/cm^2)	Reference
Activated Carbon + 10% Pt	3% PVA-PAA (30 µm)	Activated Carbon	0.1%	Air	1.4	[60]
Activated Carbon + Pt-Bi (540 µm)	Polypropylene (90 µm)	Activated carbon (400 µm)	0.1 %	Air	3.5	[12]
Pt (25 nm)	Polypropylene (50 µm)	Activated Carbon (200 µm)	0.1%	Air	1.1	This Study
Pt (25 nm)	Polypropylene (50 µm)	Graphene (185 µm)	0.1 %	Air	2.1	This Study
Pt (25 nm)	NP Silica (278 nm)	Graphene (185 µm)	0.1%	Air	5.3	This Study
Pt (25 nm)	Polypropylene (50 µm)	Activated Carbon (200 µm)	0.42%	Air	3.5	This Study
Pt (25 nm)	Polypropylene (50 µm)	Graphene (175 µm)	0.42%	Air	5.0	This Study
Pt (25 nm)	NP Silica (270 nm)	Graphene (175 µm)	0.42%	Air	6.25	This Study
Activated Carbon + 5%Pt + 5% Bi (480 µm)	Polyether-sulfone (140 µm)	Activated Carbon (480 µm)	0.1%	4 %	3.3	[48]

The power densities reported in the present study obtained from activated carbon (1.1

$\mu W/cm^2$) based BFC are lower compared values reported by Kerzenmacher et al. (~ 2 $\mu W/cm^2$)[48]. Lower power densities could be due to the reduced thickness of electrodes such as activated carbon cathode (200 µm) used in the present study compared to most of other studies employing thicker cathodes (400-800 µm) [23]. Carbon based cathodes help remove the oxygen from the incoming mixture of glucose and oxygen. Hence optimal cathode thickness is necessary to ensure anaerobic environment at the anode. Thus reduction in the membrane thickness can play a pivotal role in the overall reduction of the iBFC thickness without compromise in performance.

3.3.6 PERFORMANCE OF *IN-VIVO* IBFC

The potential of Pt/NP/G was further demonstrated by the *in-vivo* experiments. **Figure 16** shows the performance of the device when implanted. In comparison, the implanted device performed much better *in-vivo* (10 $\mu W/cm^2$, **Figure 16**) than *in-vitro* (6 $\mu W/cm^2$, **Figure 15**) due to the six times lower oxygen concentration in venous blood and high blood flow rates. The total time of the study was 12 minutes before the pig died. In another experiment extending over 50 mins, deposition of blood clots and fibrinogenic coating was noticed on the surface of the device (**Figure 17**). However, the device continued to deliver constant power output over the period of 50 minutes because glucose is diffusible through clots, suggesting operation will be successful in the presence of neo-intima.

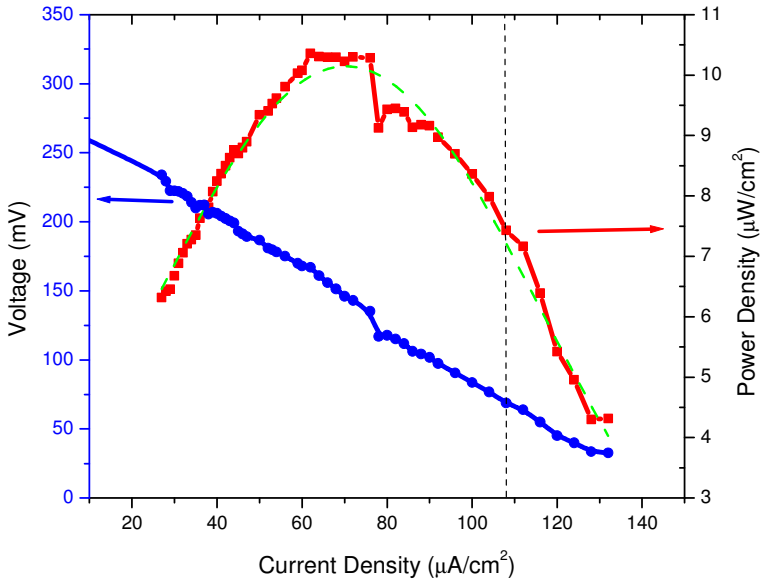

Figure 16: Plot for in-vivo studies showing the high power density obtained from iBFC

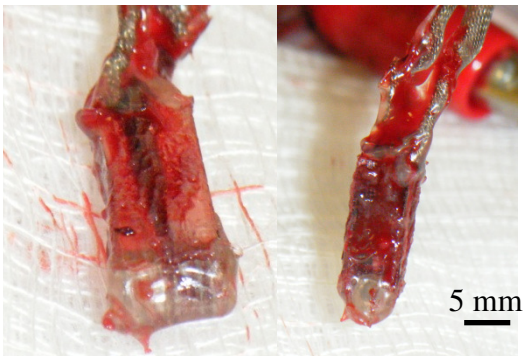

Figure 17: Photograph of the device after removal from the heart of the animal showing blood clots and fibrinogenic deposition on the entire device surface

4. DISCUSSIONS

Many studies have focused on the development of enzymatic biofuel cells using immobilized enzymes for anodes and/or cathodes. High power densities in the mW/cm^2 ranges have been reported from such systems [24, 30, 61]. However, numerous problems are associated with the usage of enzyme based iBFCs. Effective transport of electrons from the site of catalysis to electrode surface, durability of enzymes under physiological conditions and operational pH ranges, biocompatibility of enzymes and electron mediators and sterilization challenges still remain largely unaddressed. Irrespective of the type of biofuel cell, a major advantage of tissue-implanted biofuel cells is that their implantation is surgically less challenging [23]. The current study reports a viable solution to the aforementioned problems. The iBFC presented in our study presents an attractive alternative to enzymatic biofuel cells in terms of sterility, biocompatibility, stability and performance. The use of inorganic materials in the construction of the current iBFC negates the problem of delamination and sterilization. The autoclaving results corroborate this fact. Although the biocompatibility of graphene has not been proven yet, the precursor material, graphene paper, has been documented to be biocompatible [62]. With the use of nanoporous silica, we have also addressed the problem commonly encountered with most other polymeric membranes used in iBFCs of swelling and pus accumulation. Further, selective functionalization of nanoporous silica may promote glucose diffusion for the creation of better, more efficient iBFCs.

Contact angle measurements showed that the surfactant-coated polypropylene membrane was hydrophobic in nature. Hydrophobicity may have been due to degradation of the surfactant coating, which makes the surface hydrophilic for rapid wetting. It was anticipated that Pt/NP/G would perform better than Pt/PP/G iBFC due to the weakly ionic nature of the NP silica structure. Ionic conductive membranes are desired for effective diffusion of the fuel and its reaction product to and from the anode [23]. With appropriate functionalization of the surface and the pore walls, the hydrophilicity of the membrane can be precisely controlled to give the desirable membrane in ultra-thin format. The significantly higher open circuit potential of Pt/NP/G can be attributed to the ability of NP silica membrane in limiting oxygen crossover.

The power performance of the presented iBFCs were considerably higher than other literature values (**Table 5**) indicating the contribution of graphene and NP silica towards increasing the power output. Moreover, the iBFCs described here were tested under a 21% oxygen saturation condition. At physiological levels of oxygen saturation (5%), even higher power densities can be expected from the same iBFCs. An example of this would be the in-vivo performance of the Pt/NP/G iBFC which showed a power density as high as 10 $\mu W/cm^2$ - the highest power density obtained so far for an iBFC based on inorganic metal catalysts. With such a high power density output, the lifetime of a pacemaker (**Table 1**) can be extended from 7 yrs to 12 yrs. However, long duration experiments need to be performed to confirm the continuous performance of the iBFC over such time scales. Other studies have shown functional capability of iBFC *in-vitro* for

235 days and *in-vivo* up to 150 days. No reports are given of chronic implanted iBFC in blood vessels. I anticipate that devices implanted in blood vessels are subject to both greater glucose levels and neo-intimal tissue thicknesses. An important objective is to evaluate the chronic performance of an intra-vascular implanted iBFC.

We have also taken into consideration the surgical problems associated with an intra-vascular iBFC. The most common problems with conventional design of intra-vascular iBFCs are: (1) bulky nature of iBFC that can hinder the blood flow; and (2) mechanical stability [23]. Use of advanced nanomaterials can allow fabrication of ultra-thin iBFC capable of delivering very high power densities, which was not feasible for earlier iBFC designs. Further, the layered-structure can be transferred to a stent shaped platform, stent material itself acting as the anode. By creating a venous implant, the iBFC would be subjected to reduced rheological pressure conditions. When compared to arteries, large veins carry deoxygenated blood even though the glucose levels are almost equivalent [23]. Hence fabricating an ultra-thin iBFC on top of a venous stent would be a viable solution for the problems encountered by iBFCs. An added advantage of using of a stent as the supporting base is the convenience of using stents in surgical procedures. The long term aim is to enable creation of efficient, ultra-thin implantable Biofuel Cells (iBFCs) which could be mounted on stents and deployed in veins

5. CONCLUSIONS

We presented results on the use of nanoporous silica as a functional membrane and graphene as cathode for the fabrication of an ultra-thin implantable biofuel cells. Load characteristics were measured for the assembled iBFCs and showed the potential of using nanoporous silica as a membrane for an iBFC. We also observed higher current densities from the nanoporous silica based iBFC than 3 $\mu W/cm^2$. Further experiments need to be completed to establish the significant advantages of using NP silica along with its optimization. As nanoporous silica and graphene processing are becoming semiconductor clean-room friendly, the future holds great promise for the development of mass-producible, high power-density, ultra-thin biofuel cells for biomedical implant applications.

6. REFERENCES

1. Writing Group, M., et al., *Heart Disease and Stroke Statistics--2009 Update: A Report From the American Heart Association Statistics Committee and Stroke Statistics Subcommittee.* Circulation, 2009. **119**(3): p. e21-181.
2. Cho, S. and C. Kang, *Nonenzymatic glucose detection with good selectivity against ascorbic acid on a highly porous gold electrode subjected to amalgamation treatment.* Electroanalysis, 2007. **19**(22): p. 2315-2320.
3. Clauwaert, P., et al., *Minimizing losses in bio-electrochemical systems: the road to applications.* Applied Microbiology and Biotechnology, 2008. **79**(6): p. 901-913.
4. Dargahi, J., *A piezoelectric tactile sensor with three sensing elements for robotic, endoscopic and prosthetic applications.* Sensors and Actuators A: Physical, 2000. **80**(1): p. 23-30.
5. Lisichkin, G.V. and A.A. Kudrinskii, *Grafted surface compounds in chemical sensors and biosensors.* Russian Journal of General Chemistry, 2007. **77**(3): p. 325-335.
6. Lu, X.B., et al., *Carbon nanofiber-based composites for the construction of mediator-free biosensors.* Biosensors & Bioelectronics, 2008. **23**(8): p. 1236-1243.

7. Melde, B.J., B.J. Johnson, and P.T. Charles, *Mesoporous silicate materials in sensing.* Sensors, 2008. **8**(8): p. 5202-5228.

8. Najafi, N. and A. Ludomirsky, *Initial animal studies of a wireless, batteryless, MEMS implant for cardiovascular applications.* Biomedical Microdevices, 2004. **6**(1): p. 61-65.

9. Sokhanvar, S., M. Packirisamy, and J. Dargahi, *MEMS Endoscopic Tactile Sensor: Toward In-Situ and In-Vivo Tissue Softness Characterization.* Ieee Sensors Journal, 2009. **9**(12): p. 1679-1687.

10. Zhang, J. and J. Zhu, *A novel amperometric biosensor based on gold nanoparticles-mesoporous silica composite for biosensing glucose.* Science in China Series B: Chemistry, 2009. **52**(6): p. 815-820.

11. Chau, H.L. and K.D. Wise, *An Ultraminiature Solid-State Pressure Sensor for a Cardiovascular Catheter.* IEEE Transactions on Electron Devices, 1988. **35**(12): p. 2355-2362.

12. F. von Stetten, S.K., R. Sumbharaju, R. Zengerle, and J. Ducrée. *Biofuel cells as micro power generators for implantable devices*. in *Proc. Eurosensors XX*. 2006.

13. Medmovie.com, *Medmovie 2004 Cardiac Illustration*, in *medmovie.com*, 0057iStent, Editor. 2004: Lexington.

14. Appleby, A.J., D.Y.C. Ng, and H. Weinstein, *Parametric study of the anode of an implantable biological fuel cell.* Journal of Applied Electrochemistry, 1971. **1**(2): p. 79-90.

15. Appleby, A.J. and C. Van Drunen, *Anodic Oxidation of Carbohydrates and Related Compounds in Neutral Saline Solution.* Journal of The Electrochemical Society, 1971. **118**(1): p. 95-97.

16. Kreysa, G., D. Sell, and P. Kramer, *Bioelectrochemical Fuel-Cells.* Berichte Der Bunsen-Gesellschaft-Physical Chemistry Chemical Physics, 1990. **94**(9): p. 1042-1045.

17. Rao, J.R., et al., *Performance of Glucose Electrodes and Characteristics of Different Biofuel Cell Constructions.* Bioelectrochemistry and Bioenergetics, 1976. **3**(1): p. 139-150.

18. Mele, M.F.L.D., M.J. Cardos, and H.A. Videla, *A Biofuel Cell as a Bioelectrochemical Sensor of Glucose-Oxidation.* Anales De La Asociacion Quimica Argentina, 1979. **67**(4): p. 125-138.

19. Weidlich, E., et al., *Animal-Experiments with Bio-Galvanic and Bio-fuel Cells.* Biomaterials Medical Devices and Artificial Organs, 1976. **4**(3-4): p. 277-306.

20. Ramanavicius, A., A. Kausaite, and A. Ramanaviciene, *Biofuel cell based on direct bioelectrocatalysis.* Biosensors & Bioelectronics, 2005. **20**(10): p. 1962-1967.

21. Prauer, H.W., et al., *Lithium-Powered Cardiac-Pacemakers.* Medizinische Klinik, 1977. **72**(44): p. 1885-1891.

22. Cinquin, P., et al., *A Glucose BioFuel Cell Implanted in Rats.* PLoS ONE. **5**(5): p. e10476-e10476.

23. Kerzenmacher, S., et al., *Energy harvesting by implantable abiotically catalyzed glucose fuel cells.* Journal of Power Sources, 2008. **182**(1): p. 1-17.

24. Fernandez, J.L., et al., *Optimization of "wired" enzyme O-2-electroreduction catalyst compositions by scanning electrochemical microscopy.* Angewandte Chemie-International Edition, 2004. **43**(46): p. 6355-6357.

25. Mano, N., *A miniature membrane-less biofuel cell operating at+0.60 V under physiological conditions.* Abstracts of Papers of the American Chemical Society, 2005. **230**: p. U1661-U1661.

26. Minteer, S.D., B.Y. Liaw, and M.J. COoney, *Enzyme-based biofuel cells.* Current Opinion in Biotechnology, 2007. **18**(3): p. 228-234.

27. Boland, S., et al., *Biocatalytic fuel cells: A comparison of surface pre-treatments for anchoring biocatalytic redox films on electrode surfaces.* Journal of Electroanalytical Chemistry, 2009. **626**(1-2): p. 111-115.

28. Rao, J.R., *Bioelectrochemistry. I. Biological Redox Reactions,*, M.B. G. Milazzo, Editor. 1983,, Plenum Press, New York. p. 283–335.

29. A. Kloke, B.B., S. Kerzenmacher, U. Kräling, R. Zengerle, and F. von Stetten. *A single layer biofuel cell as potential coating for implantable low power devices*. in *Eurosensors Proceedings*. 2008.

30. Bartlett, P.N. and E. Simon, *Poly(aniline)-poly(acrylate) composite films as modified electrodes for the oxidation of NADH.* Physical Chemistry Chemical Physics, 2000. **2**(11): p. 2599-2606.

31. Chen, T., et al., *A miniature biofuel cell.* Journal of the American Chemical Society, 2001. **123**(35): p. 8630-8631.

32. Saffarian, H.M., et al., *Acceleration of oxygen reduction rate by alkyl derivatives of uracil on Pt catalysts used in fuel cells.* Journal of the Electrochemical Society, 2001. **148**(6): p. A559-A564.

33. Tsujimura, S., K. Kano, and T. Ikeda, *Glucose/O-2 biofuel cell operating at physiological conditions.* Electrochemistry, 2002. **70**(12): p. 940-942.

34. Mano, N., et al., *An oxygen cathode operating in a physiological solution.* Journal of the American Chemical Society, 2002. **124**(22): p. 6480-6486.

35. Wong, T.S. and U. Schwaneberg, *Protein engineering in bioelectrocatalysis.* Current Opinion in Biotechnology, 2003. **14**(6): p. 590-596.

36. Soukharev, V., N. Mano, and A. Heller, *A four-electron O-2-electroreduction biocatalyst superior to platinum and a biofuel cell operating at 0.88 V.* Journal of the American Chemical Society, 2004. **126**(27): p. 8368-8369.

37. Barriere, F., P. Kavanagh, and D. Leech, *A laccase-glucose oxidase biofuel cell prototype operating in a physiological buffer.* Electrochimica Acta, 2006. **51**(24): p. 5187-5192.

38. Furukawa, Y., T. Moriuchi, and K. Morishima, *Design principle and prototyping of a direct photosynthetic/metabolic biofuel cell (DPMFC).* Journal of Micromechanics and Microengineering, 2006. **16**(9): p. S220-S225.

39. Habrioux, A., et al., *Concentric glucose/O-2 biofuel cell.* Journal of Electroanalytical Chemistry, 2008. **622**(1): p. 97-102.

40. Zebda, A., et al., *A microfluidic glucose biofuel cell to generate micropower from enzymes at ambient temperature.* Electrochemistry Communications, 2009. **11**(3): p. 592-595.

41. Colmati, F., et al., *Enzymatic based biocathode in a polymer electrolyte membrane fuel cell.* International Journal of Electrochemical Science, 2007. **2**(2): p. 195-202.

42. Kang, C., H. Shin, and A. Heller, *On the stability of the "wired" bilirubin oxidase oxygen cathode in serum.* Bioelectrochemistry, 2006. **68**(1): p. 22-26.

43. Beltzer, M.B., J. S. *Limitations of blood plasma as a fuel cell electrolyte*. in *Proc. Intersoc. Energy Convers. Eng. Conf., 4th*. 1969.

44. Barton, S.C. and P. Atanassov, *Enzymatic biofuel cells for implantable and micro-scale devices.* Abstracts of Papers of the American Chemical Society, 2004. **228**: p. 004-FUEL.

45. Bruno, M.M., et al., *Electrodeposited platinum catalysts over hierarchical carbon monolithic support.* Journal of Applied Electrochemistry, 2009. **40**(2): p. 257-263.

46. Habrioux, A., et al., *Activity of platinum-gold alloys for glucose electrooxidation in biofuel cells.* Journal of Physical Chemistry B, 2007. **111**(34): p. 10329-10333.

47. Jin, C. and Z. Chen, *Electrocatalytic oxidation of glucose on gold-platinum nanocomposite electrodes and platinum-modified gold electrodes.* Synthetic Metals, 2007. **157**(13-15): p. 592-596.

48. Kerzenmacher, S., et al., *An abiotically catalyzed glucose fuel cell for powering medical implants: Reconstructed manufacturing protocol and analysis of performance.* Journal of Power Sources, 2008. **182**(1): p. 66-75.

49. Gebhardt, U.R., J.R.; Richeter, G.J., *A Special Type of Raney-alloy catalyst used in compact Biofuel Cells.* Journal of Applied Electrochemistry, 1976. **6**: p. 127-134.

50. Gupta, G., et al., *Highly Stable and Active Pt−Cu Oxygen Reduction Electrocatalysts Based on Mesoporous Graphitic Carbon Supports.* Chemistry of Materials, 2009. **21**(19): p. 4515-4526.

51. Kloke, A.K., S.; Zengerle, R., Stetten, F. von, *Electrodeposited thin-layer electrodes for he use in Potentially implantable Glucose Fuel cells*, in *Transducers*. 2009: Denver, CO, USA. p. 537-540.

52. Stoller, M.D., et al., *Graphene-Based Ultracapacitors.* Nano Letters, 2008. **8**(10): p. 3498-3502.

53. Choi, Y.K., et al., *A hybrid biofuel cell based on electrooxidation of glucose using ultra-small silicon nanoparticles.* Biosensors & Bioelectronics, 2009. **24**(10): p. 3103-3107.

54. Shi, B., S. Sinha, and V.K. Dhir. *Molecular simulation of the contact angle of water droplet on a platinum surface*. in *ASME International Mechanical Engineering Congress and Exposition, Novement 5*. 2005.

55. Hu, Y.B., Ali; Liu, Xuewu; Tasciotti, Ennio; Li, Li; Ferrari, Mauro. *The next generation of proteomic nanochips in biomarker discovery*. in *Nanotech Conference & Expo 2009: An Interdisciplinary Integrative Forum on Nanotechnology, Biotechnology and Microtechnology*. 2009.

56. Bouamrani, A., et al., *Mesoporous silica chips for selective enrichment and stabilization of low molecular weight proteome.* Proteomics, 2009. **10**(3): p. 496-505.

57. Hu, Y., et al., *Tailoring of the Nanotexture of Mesoporous Silica Films and Their Functionalized Derivatives for Selectively Harvesting Low Molecular Weight Protein.* ACS Nano, 2010. **4**(1): p. 439-451.

58. Airoldi, F., et al., *Comparison of diamond-like carbon-coated stents versus uncoated stainless steel stents in coronary artery disease.* The American Journal of Cardiology, 2004. **93**(4): p. 474-477.

59. Qu, D., *Investigation of oxygen reduction on activated carbon electrodes in alkaline solution.* Carbon, 2007. **45**(6): p. 1296-1301.

60. Stetten, F.v.K., S; Lorenz, A.; Chokkalingam, V.; Miyakawa, N.; Zengerle, R.; Ducree, J., *A One-Compartment, Direct Glucose Fuel Cell for Powering Long-term Medical Implants*, in *MEMS 2006*. 2006, IEEE: Istanbul, Turkey. p. 934-937.

61. Komaba, S., T. Mitsuhashi, and S. Shiraishi, *Polyion complex nanocomposite electrode incorporating enzyme and carbon nanotube for biofuel cells.* Electrochemistry, 2008. **76**(1): p. 55-58.

62. Chen, H., et al., *Mechanically Strong, Electrically Conductive, and Biocompatible Graphene Paper.* Advanced Materials, 2008. **20**(18): p. 3557-3561.

VITA

Tushar Sharma was born in Mandi, a small town in the valleys of Himachal Pradesh, India. He did his undergraduate studies in the Biotechnology Department at The Indian Institute of Technology Madras, India. He graduated with a Bachelors in Technology from Indian Institute of Technology Madras in June 2008. He also received the prestigious Bhagyalakshmi and Ayengar Award for the best B. Tech. Thesis. In August 2008, he entered the Graduate School at The University of Texas at Austin.

Permanent Address: Flat No 6, Shivmala Apts
Makarpura Road, Vadodara – 09
Gujarat, India

This thesis was typed by the author